Recorded Earthquake Responses from the Integrated Seismic Monitoring Network of the Atwood Building, Anchorage, Alaska

Mehmet Çelebi,[a] **M.EERI**

An integrated seismic monitoring system with a total of 53 channels of accelerometers is now operating in and at the nearby free-field site of the 20-story steel-framed Atwood Building in highly seismic Anchorage, Alaska. The building has a single-story basement and a reinforced concrete foundation without piles. The monitoring system comprises a 32-channel structural array and a 21-channel site array. Accelerometers are deployed on 10 levels of the building to assess translational, torsional, and rocking motions, interstory drift (displacement) between selected pairs of adjacent floors, and average drift between floors. The site array, located approximately a city block from the building, comprises seven triaxial accelerometers, one at the surface and six in boreholes ranging in depths from 15 to 200 feet (~5–60 meters). The arrays have already recorded low-amplitude shaking responses of the building and the site caused by numerous earthquakes at distances ranging from tens to a couple of hundred kilometers. Data from an earthquake that occurred 186 km away traces the propagation of waves from the deepest borehole to the roof of the building in approximately 0.5 seconds. Fundamental structural frequencies [0.58 Hz (NS) and 0.47 Hz (EW)], low damping percentages (2–4%), mode coupling, and beating effects are identified. The fundamental site frequency at approximately 1.5 Hz is close to the second modal frequencies (1.83 Hz NS and 1.43 EW) of the building, which may cause resonance of the building. Additional earthquakes prove repeatability of these characteristics; however, stronger shaking may alter these conclusions.
[DOI: 10.1193/1.2359702]

INTRODUCTION

The Atwood Building, designed according to 1979 *Uniform Building Code* (*UBC*) and constructed in 1980, is located in highly seismic Anchorage, Alaska. The 20-story-tall building (Figure 1) is a steel moment-resisting framed (MRF) structure with only one level of basement, 130 × 130 ft (39.6 m × 39.6 m) in plan with a 48 × 48-ft (14.6 × 14.6-m) in-plan center steel shear-walled core, and 264 ft (80.5 m) tall. The building foundation is without any piles and consists of a 5-ft (1.52-m) thick reinforced-concrete mat below the core and a 4-ft 6-in. (1.37-m) thick reinforced-concrete perimeter mat interconnected with grade beams.

[a] Research Civil Engineer, Earthquake Hazards Team, U.S. Geological Survey, Menlo Park, CA 94025

Earthquake Spectra, Volume 22, No. 4, pages 847–864, November 2006; © 2006, Earthquake Engineering Research Institute

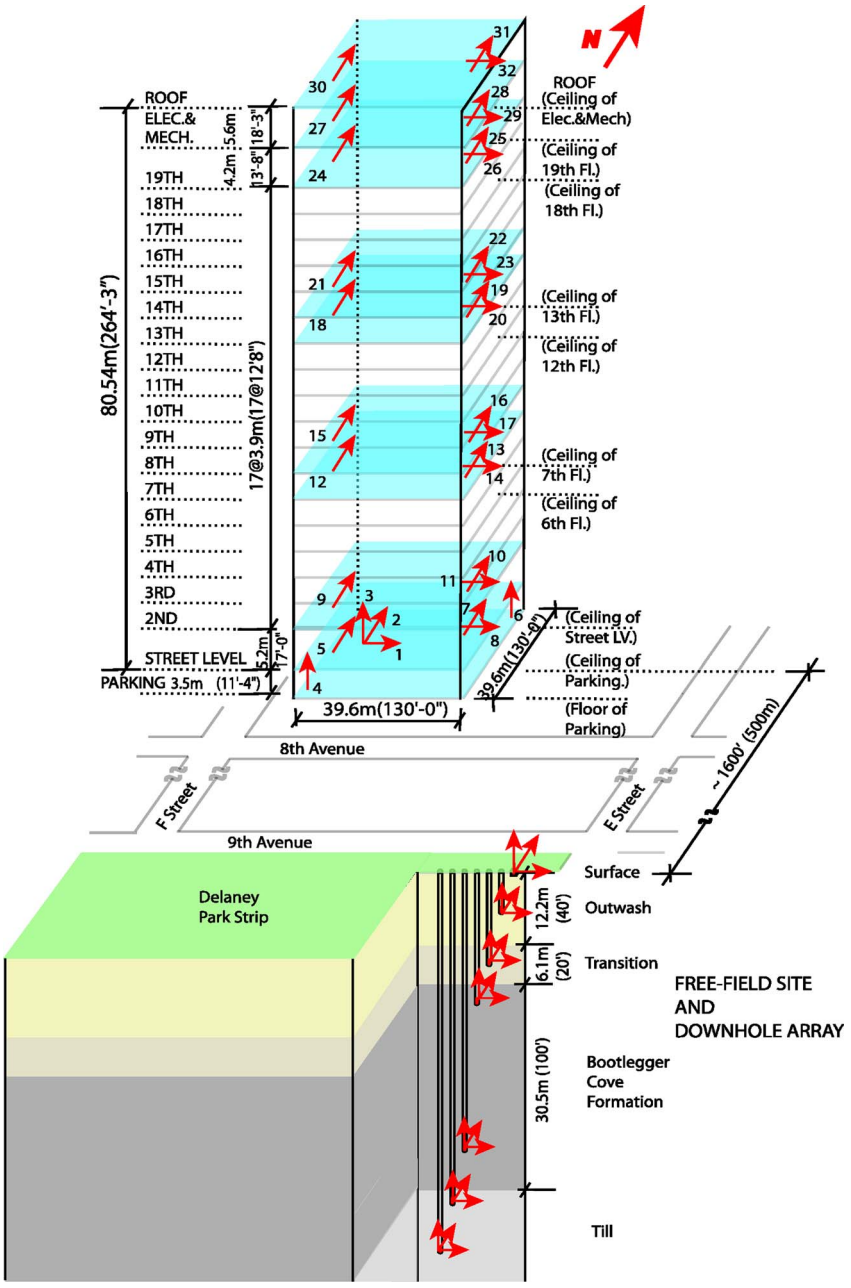

Figure 1. Three-dimensional schematic of the Atwood Building (Anchorage, Alaska) showing the general dimensions and locations of accelerometers deployed within the structure and in the free-field with tri-axial downhole accelerometers. The sub-arrays (e.g., superstructure, foundation, surface, and downhole free-field sub-arrays) of this particular building monitoring scheme are designed to capture (rocking) SSI effects in addition to the traditional translational and torsional responses.

The site of the building in downtown Anchorage is underlain by an approximately 100–150-feet (30.5–45.7-m) thick soil layer known as the Bootlegger Cove Formation, where considerable ground failures occurred during the 1964 Great Alaska earthquake (Updike and Carpenter 1986). The Atwood Building was selected for seismic monitoring because recording responses and then assessing the behavior of this building and its site during earthquakes of various levels of shaking can enhance seismic assessment of the behavior and performances of similar buildings in similar geotechnical and seismic environment during future large earthquakes.

In general, an instrumented structure should provide enough information to (1) reconstruct the response of the structure in sufficient detail to compare with the response predicted by mathematical models and those observed in laboratories, the goal being to improve the models; (2) make it possible to explain the reasons for any damage to the structure; and (3) facilitate decisions to retrofit/strengthen the structural systems when warranted. In addition, a structural array should include, if physically possible, an associated free-field triaxial accelerograph so that the interaction between soil and structure can be quantified (Çelebi 2000, 2001, 2004b). Recent trends in development of performance-based earthquake-resistant design methods and related needs of the engineering community and owners to rapidly and informedly assess functionality of a building following an event, as well as advances in computation, communication, and data transmission capabilities, have prompted development of new approaches for structural monitoring issues and applications. Such an application has been described and implemented by Çelebi et al. (2004).

The seismic monitoring system of the building comprises and integrates a structural (superstructure and foundation) array and a site (surface and downhole) array (Figure 1). The superstructure and foundation array, designed by the author, consists of accelerometers deployed on the basement, at street level, and on the 2nd, 7th, 8th, 13th, 14th, and 19th floors (Çelebi 2003). This configuration is designed to detect lateral north-south (NS) and east-west (EW) motions throughout the building, and vertical motions in the basement to assess (a) translational motion, (b) torsional motion, (c) interstory drift (displacement between selected two consecutive floors) or average drift between any two floors, and (d) rocking of the building. The structural array is complemented by an extensive free-field site array, located approximately one city block south of the building, and consisting of seven triaxial accelerometers, one at the surface and six in boreholes with depths ranging from 15 to 200 feet (5 to 60 m)(Figure 1). Removed from the vibrational effects of the building, the associated site array is designed to capture the response of varying layers of soil, and how such layering alters the characteristics of earthquake motions as they travel to the surface and shake the structure. Thus, with the integrated site and superstructure arrays, propagation of motions starting from the deepest downhole to the ground surface, basement, and roof of the building are recorded to facilitate structural, site response, and soil-structure interaction (SSI) studies. Capturing the propagation and travel time is important, as large and abrupt changes may indicate damage to structural members, components, and the system (Safak 1999).

The arrays were deployed in 2003. Since then, numerous small and medium-size earthquakes from near and far sources (Table 1 and Figure 2) have been recorded. The

Table 1. Earthquakes recorded by the Atwood Building Seismic Monitoring System. Coordinates of the building: 61.21528 latitude and 149.89296 longitude.

Event No.	Date	OT UTC	Event	Lat.	Long.	H km	M	Dist. km	Azim.*
1	2003/12/15	14:55	Pt. MacKenzie	61.350	−149.687	37	3.7	19	36
2	2004/03/25	21:30	Anchorage	61.146	−149.188	30	3.7	39	101
3	2004/04/23	04:47	Pt. MacKenzie	61.425	−149.889	41	3.8	23	1
4	2004/05/30	11:03	Tyonek	61.076	−152.217	128	5.3	126	264
5	2004/06/21	19:44	Talkeetna	62.084	−150.038	43	4.4	97	356
6	2004/06/21	21:29	Skwentna	61.653	−151.255	81	5.2	88	304
7	2004/08/23	07:19	Willow	61.811	−149.909	43	3.8	66	359
8	2004/09/21	03:25	SE Anchorage	61.100	−149.719	32	3.1	16	144
9	2004/10/17	21:12	Beluga	61.209	−150.850	60	4.3	51	270
10	2004/11/08	06:21	Denali Park	63.076	−151.425	9	4.9	222	340
11	2004/12/09	06:35	Pt. MacKenzie	61.347	−150.207	41	3.5	22	311
12	2004/12/21	17:21	Knight Island	60.448	−147.549	1	5.1	153	123
13	2005/01/13	17:36	Knight Island	60.465	−147.547	10	4.7	153	122
14	2005/02/16	18:35	Pt. MacKenzie	61.337	−149.845	35	4.7	14	11
15	2005/02/16	18:41	Pt. MacKenzie	61.304	−149.862	36	3.9	10	10
16	2005/02/16	19:52	Pt. MacKenzie	61.300	−149.792	30	3.3	11	30
17	2005/03/16	10:53	Pt. MacKenzie	61.300	−149.792	30	3.6	11	30
18	2005/04/06	17:51	Tazlina Glacier	61.454	−146.518	17	4.9	183	80
19	2005/07/27	07:00	Sunrise, Kenai	60.818	−149.410	35	3.8	51	149

Not all of the data from all events are processed. Those processed and documented are available at the web site of the USGS National Strong Motion Program Data Center (nsmp.wr.usgs.gov).
* Azim. = Azimuthal Angle (clockwise from north) to the earthquake

low-amplitude shaking of the building caused by these earthquakes did not result in any damage, but provides opportunities to identify response characteristics of the building and the site. Yang and others (2004) performed studies of only the data from the building array. This paper introduces and analyzes recorded data from both structural and site arrays. We select three earthquakes (events 10, 14, and 18 in Table 1 and Figure 2) to gain insight into the response of the building to distant and near earthquakes: event 10, originating north of the building at 222 km distance; event 18, originating east of the building at 183 km distance; and event 14, originating north of the building at 14 km distance. Data from event 18 are analyzed in detail. Data from all three events are compared to affirm repeatability of the important building and site responses to earthquakes from a range of distances. In particular, repeatability is important to confirm if the beating and resonating behavior of the building observed in the detailed analyses for event 18 also occurs in the other two events. Beating occurs when repetitively stored potential energy during the coupled translational and torsional deformations turns into repetitive vibrational energy. The energy flows back and forth between closely coupled modes.

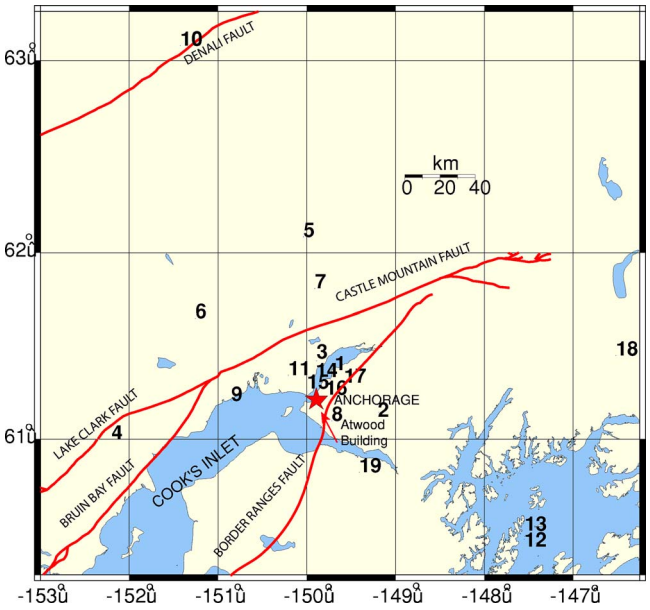

Figure 2. Location of the Atwood Building in Anchorage, Alaska, and the major faults in the region. Numbers correspond to events (summarized in Table 1).

Thus periodic, repeating, and resonating motions ensue. Beating can become severe if the system is lightly damped (Çelebi 2004a). Due to low-amplitude shaking, drift ratio studies are not included in this paper.

Throughout the paper, spectral analyses described by Bendat and Piersol (1980) and system identification procedures described by Ljung (1997) are used.

ANALYSES OF STRUCTURAL AND SITE ARRAY DATA: EARTHQUAKE OF 6 APRIL 2005

TIME HISTORIES AND WAVE PROPAGATION

Acausally filtered accelerations and computed displacements (double-integrated accelerations) from both the site and the superstructure arrays of the Atwood Building during the 6 April 2005 Tazlina Glacier (Alaska) earthquake (M_L=4.9, event 18), epicenter at 183 km from the building, are shown in Figures 3 and 4. The largest peak acceleration recorded in the building array is on the order of 0.5% g. The figures clearly show the propagation of waves from the basement to the roof of the building. The height of this building is 264 ft (~81 m) from ground floor and 275 ft (~85 m) from basement. The travel time of waves from the basement to the roof is about 0.4–0.5 seconds and, as expected because of the low-amplitude shaking, the propagation of the waves does not display abrupt changes (e.g., transients or spikes) to indicate damage to structural members, components and the overall structural system. Capturing the propagation charac-

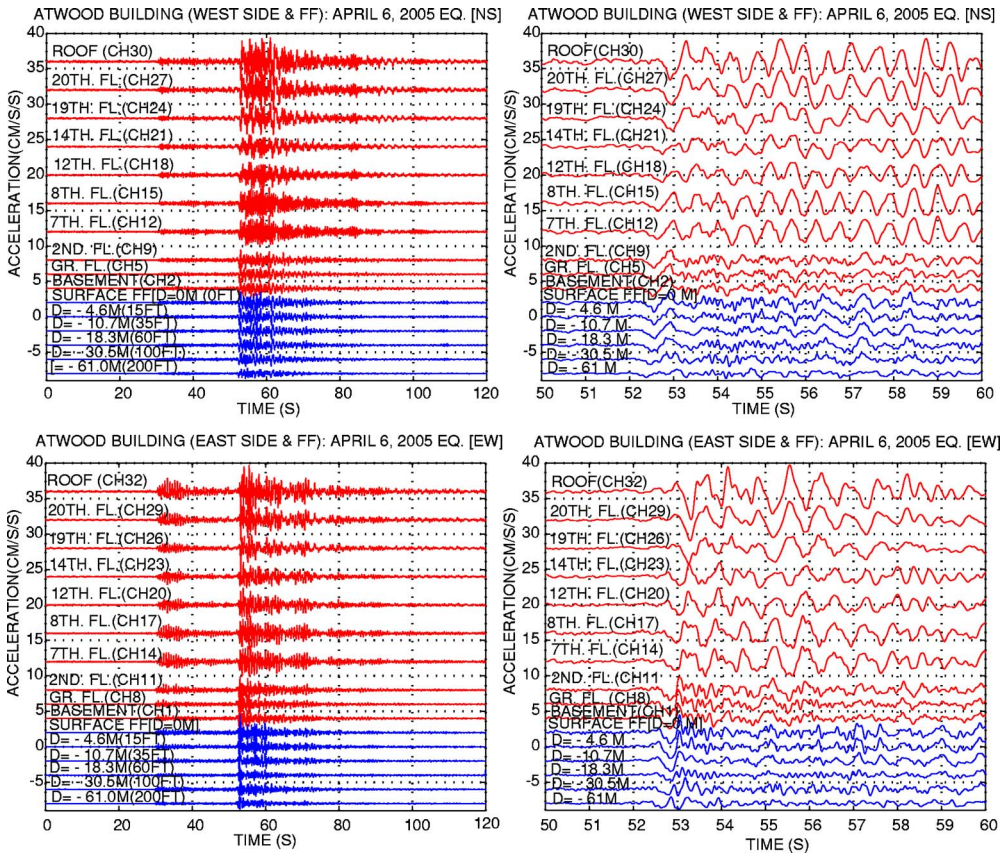

Figure 3. NS (upper panels) and EW (lower panels) accelerations from both the structure and site arrays. The 10-second records on the right are expanded views between 50 and 60 seconds of the longer records on the left, and show in detail the propagation of S wave from the deepest downhole to the roof of the building. (Note: vertical axes are not in scale with the vertical elevations.)

teristics and travel time is important, as large and abrupt changes may indicate damage to structural members, components, and the system (Safak 1999). If there are cracks in the structural system, the travel time will be longer because of the delay due to damage (Safak 1999).

In addition to displaying propagation of waves, Figure 4 also shows the beating response of the building, particularly in the NS direction displacement responses (between 80 and 100 s and also 100 and 120 s). Further beating analysis is presented later in this paper.

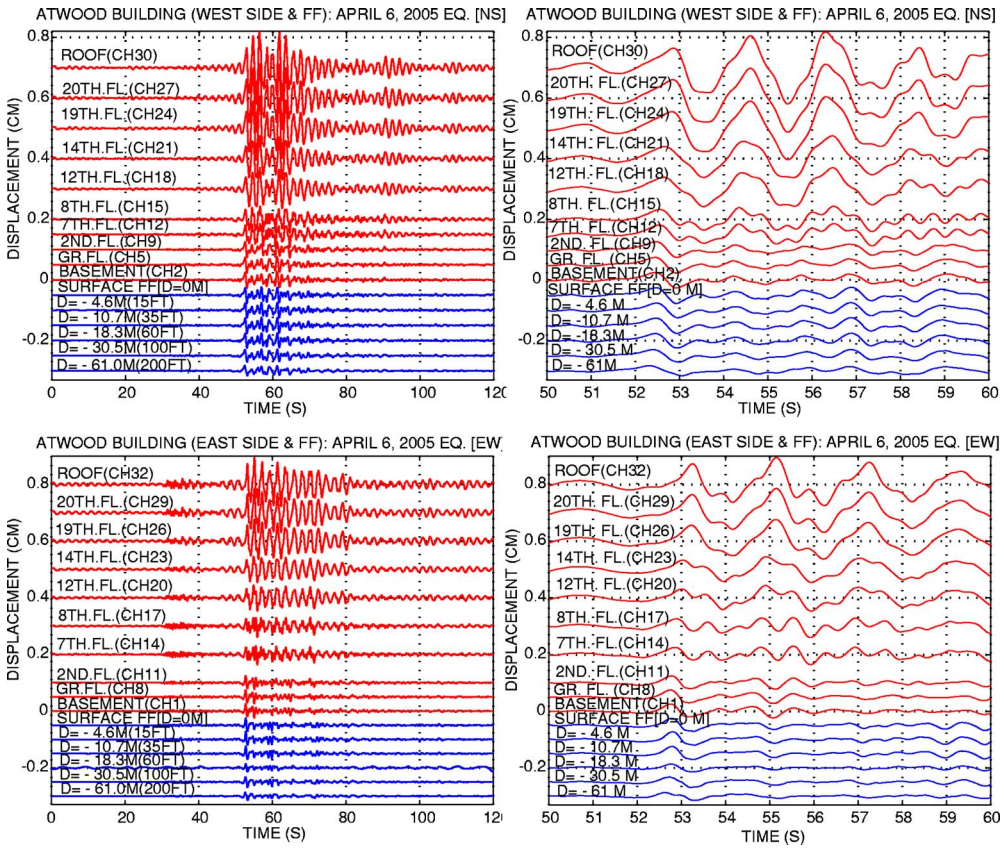

Figure 4. NS and EW displacements corresponding to Figure 3. (Note: vertical axes are not in scale with the vertical elevations.)

TRANSLATIONAL AND TORSIONAL RESPONSES OF THE BUILDING

Figure 5 shows the roof accelerations and corresponding amplitude spectra of the two parallel NS components, their difference, and the EW component. In the spectra, significant structural frequencies (NS [0.58 and 1.83 Hz] and EW [0.47 and 1.56 Hz]) are identified. These frequencies, and in particular, predominant torsional frequencies computed from differential accelerations of parallel sensors at roof level (CH30–CH31), are better displayed in Figure 6 showing spectral ratios of amplitude spectra of (a) NS and (b) EW accelerations (at the roof [CH30 and CH32] and 8th floor [CH15 and CH17] with respect to basement [CH2 and CH1], respectively), and (c) torsional accelerations at the roof [CH30–CH31] and 8th floor [CH15–CH16] with respect to those at the ground floor [CH5–CH7]. The torsional frequencies [0.47–0.58 and 1.5–1.9 Hz] computed from differential accelerations (Figure 5 and 6) are similar to the predominant frequencies computed from NS and EW roof accelerations, indicating possible coupling and also possibly causing the beating effect visually most prominent in the displacement

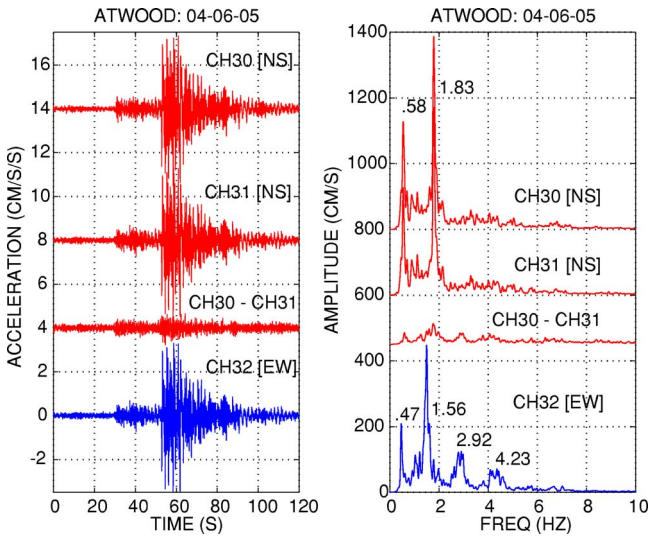

Figure 5. Roof acceleration time histories and corresponding amplitude spectra.

time-history plots (Figure 4). Furthermore, the narrow band of the structural frequencies in the amplitude spectra or the spectral ratios reflect the low damping ratios. The translational frequencies and low damping percentages are further confirmed by system identification later in the paper.

Figure 7 shows torsional acceleration time histories (computed from differential NS accelerations) for each floor from ground floor to the roof. This time history clearly indicates (a) beating effect and (b) a dominant frequency of about 1.6–1.8 Hz determined

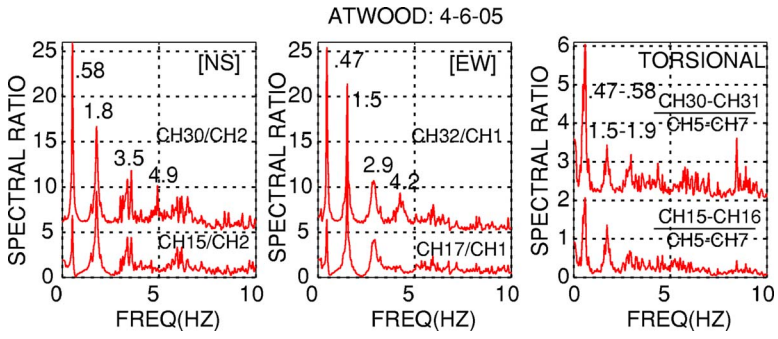

Figure 6. Spectral ratios computed from amplitude spectra of NS and EW accelerations at the roof (CH30 and CH32, respectively) and 8th floor (CH15 and CH17 with respect to those at basement, and torsional accelerations at the roof and 8th floor with respect to those at ground floor (CH5 and CH7).

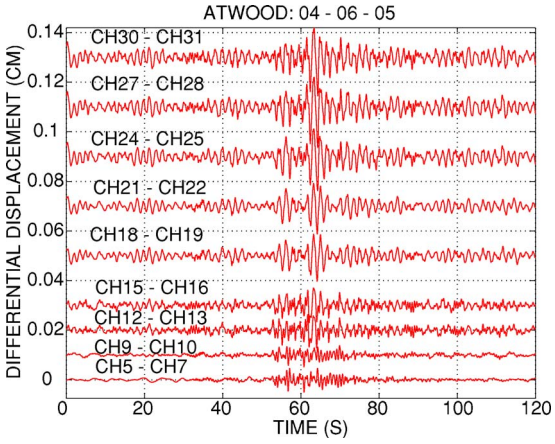

Figure 7. Torsional acceleration time histories (differential NS accelerations) on different levels of the building displays beating effect as well as a dominant frequency of about 0.55–0.60 Hz) at upper floors.

by 11–12 counts of cycles within a duration of 20 seconds (thus T=1.66–1.82 and f =0.55–0.60 Hz). This frequency is close to the NS fundamental frequency, thus inferring coupling of the translational-torsional motions.

Figure 8 presents cross spectrum, coherence, and phase angle plots of pairs at the roof and 8th floor of NS (a) CH30 and CH15, EW (b) CH32 and CH17, and torsional (differential of NS) accelerations (c) CH30–CH31 and CH15–CH17. The pairs of accelerations in each case are perfectly coherent for the modal frequencies indicated, and are 0° in phase for the lowest frequencies (indication of first mode) and 180° out of phase for the second and third lowest frequencies (indicating second and higher modes). It is noted again that the frequencies for the torsional responses are similar to the translational frequencies.

SYSTEM IDENTIFICATION

Figure 9 shows a sample system identification analysis for the NS building response. Such analysis allows computation of modal damping values in addition to the modal frequencies. The ARX (AR for autoregressive and X for extra input) model, based on the least squares method for single input-single output coded in commercially available system identification software (MathWorks 1998), is used in system identification analyses performed herein (Ljung 1997). Typically the input is the basement or ground-floor motion and the output is the roof-level motion or one of the levels where the structural response is recorded. Modes are extracted as shown in Figure 10. Essentially, the first two modes contribute most to the NS displacement of the roof (CH30). The damping ratios are extracted with the procedures outlined by Ghanem and Shinozuka (1995). The figure shows nearly perfect prediction of the roof motions. Results extracted from the analyses are summarized in Table 2, which shows that for the first two modes, the modal damping

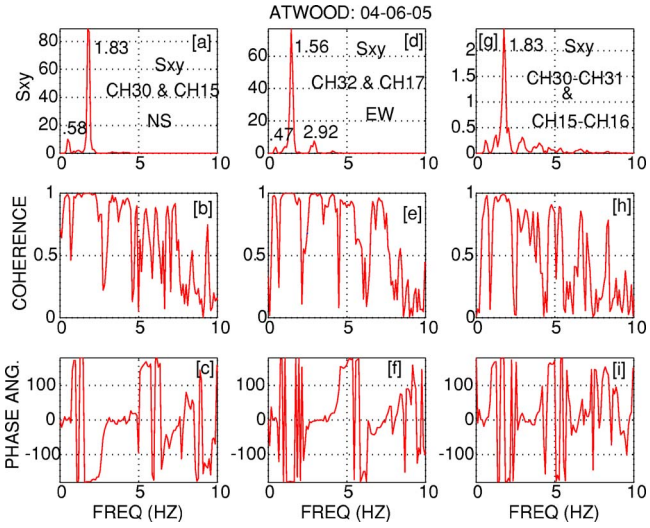

Figure 8. Cross spectrum, coherence, and phase angle plots of pairs of NS (CH30 and CH15), EW (CH32 and CH17) and differential of NS accelerations (CH30–CH31 and CH15–CH17) at the roof and 8th floor identify significant frequencies and associated modes.

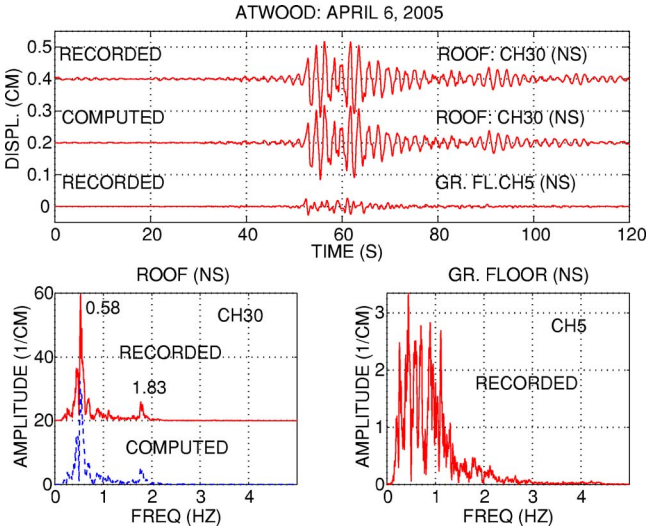

Figure 9. System identification of NS displacements (CH5 at the ground floor is used as input and CH30 as the output). The recorded and computed roof displacements and their amplitude spectra are nearly perfectly matched.

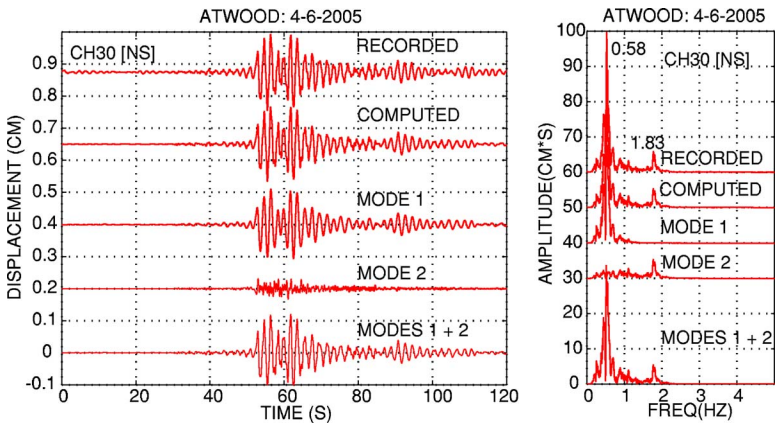

Figure 10. Time histories and corresponding amplitude spectra of recorded and computed NS displacements at the roof (CH30) with essentially modes 1 and 2 contributing to the total response. Superimposed modes 1 and 2 produce similar time history and amplitude spectra as the total response.

values are relatively low. This may be due to the low level of shaking. During stronger shaking, higher damping is expected. As a result, responses may be affected. As observed in other studies (Boroscheck et al. 1990, Boroscheck and Mahin 1991, Çelebi 1994), the low-level damping and nearly identical translational and torsional frequencies could cause the coupling and beating effect observed in Figures 4, 7, and 8. Repetitively stored potential energy during the coupled translational and torsional deformations turns into repetitive vibrational energy. The energy flows back and forth between closely coupled modes.

SITE RESPONSE

Figure 11 shows amplitude spectra of (a) NS and (b) EW accelerations in the building (roof, 8th floor, and basement) and of (c) NS and (d) EW accelerations in the basement and surface and deepest downhole free-field motions. The figure illustrates, at least below 5 Hz, that the building natural frequencies are different from those of the site.

Table 2. Dynamic characteristics determined by system identification (ξ=modal damping)

	NS			EW		
Mode	f (Hz)	T (s)	ξ (%)	f (Hz)	T (s)	ξ (%)
1	0.58	1.73	2.7	0.47	2.13	4.2
2	1.83	0.55	2.7	1.53	0.65	2.8
3	3.6	0.28	5.1	2.9	0.35	2.4
4	4.9	0.20	3.6	4.3	0.24	4.1

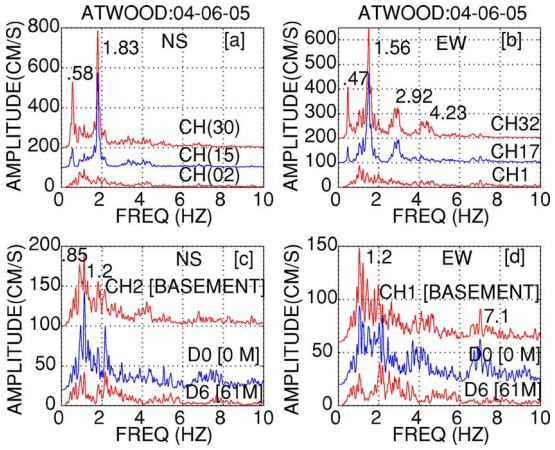

Figure 11. Amplitude spectra of (a) NS and (b) EW accelerations in the building (roof [CH30], 8th floor [CH15], and basement [CH2]), and of (c) NS and (d) EW accelerations in the basement and surface [D0], and deepest downhole [D6] free-field.

Figures 12–14 are presented to corroborate site frequencies as determined from records or computation of transfer functions using site borehole data. Figure 12 shows amplitude spectra of NS and EW accelerations and corresponding spectral ratios at basement and the free-field array computed with respect to the deepest borehole at −61 m. Significant frequency peaks identified from the figure are approximately 1.2–1.7, 4, 7, and 9.0–9.5 Hz in the NS direction and 1.5, 4.0–4.2, 7 and 9 Hz in the EW direction. It is noted that the fundamental frequency (period) [1.2–1.7 Hz (0.58–0.83 s) NS and

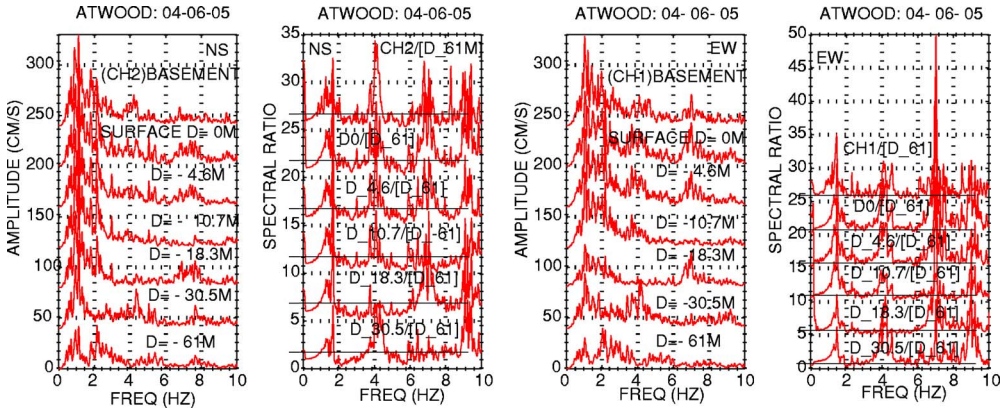

Figure 12. Amplitude spectra and corresponding spectral ratios computed from the amplitude spectra of NS and EW acceleration at basement and the free-field array computed with respect to the deepest borehole at −61 m.

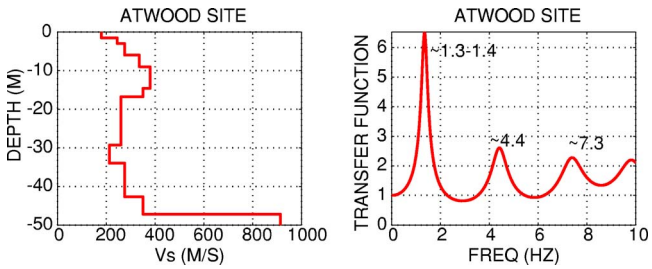

Figure 13. Shear-wave velocity (V_s) depth profile and the computed transfer function.

1.5 Hz (0.67 s) EW] at this site are not identical and appear to be azimuthally dependent. These site frequencies are consistent with those of the transfer function computed from the shear wave velocity–depth profile (D. Cole, pers. comm., 2003) at the site using software developed by Mueller (pers. comm., 2005) based on Haskell's shear-wave propagation method (Haskell 1953, 1960). In this method, the transfer function is computed using linear propagation of vertically incident SH waves and as input data related to the layered media (number of layers, depth of each layer, corresponding shear-wave velocities [Vs], damping, and density), desired depth of computation of transfer function, sampling frequency, half-space substratum shear-wave velocity, and density. Damping (ξ) in the software is provided as Q, a term used by geophysicists, and is related to damping by $\xi = 1/(2Q)$. Q values used in calculating the transfer functions are between 25 and 60 for shear-wave velocities between 200 and 600 m/s, having been approximately interpolated to vary linearly within these bounds. The resulting transfer function shows significant frequency peaks (Figure 13). Furthermore, in Figure 14, the computed transfer function is compared to the spectral ratio obtained from amplitude spectra of NS and EW accelerations at the surface with respect to downhole at 61 m depth. It can be concluded from this figure that the computed and observed transfer function are in reasonably good agreement. The often-used simple formula, $T_s = 4H/V_s$, requires minimal but reasonable characterization of depth to bedrock and representative average shear-wave velocities of layered media (*International Building Code* [ICC 2000]). Computing

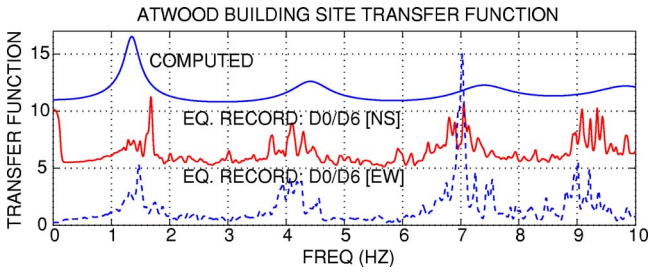

Figure 14. Comparison of computed transfer function to the spectral ratio of amplitude spectra of NS and EW accelerations at the surface with respect to downhole at 61 m depth.

average V_s=300–350 m/s using the formula $V_s(ave)=H/(\Sigma(h_i/V_{si})$, and using a depth H=50 m, then T_s=0.58–0.67 (or f_s=1.5–1.75 Hz), similar to the computed and observed site period.

No evidence of soil-structure interaction (SSI) effects was found for the low-amplitude shaking caused by this distant small earthquake. Even though the vertical motions at the basement are not identical for the three locations, no phase differences were observed. As a result, no rocking effects have been identified. Stronger shaking at the site and building from future earthquakes may reveal such effects. However, the fundamental frequency of the site (1.3–1.7 Hz) is very close to the second modal frequencies of the building (1.83 Hz for NS and ~1.5 Hz for EW directions), thus inferring that resonance of the building at this mode might occur. This is further corroborated in the next section.

REPEATABILITY

It is important to show that the significant structural behavioral aspects and responses to earthquakes are repeatable for different events whether they originate at near or far distances—mainly as proxy for different spectral shapes of input motions. It is intended herein to show that beating and site effects are repeatable for events in addition to the one studied previously.

BEATING EFFECT

Figure 15 shows NS acceleration and displacement responses of the roof (Channel 30) for the selected three events. The three events are comparable in magnitude, and although they originate at different distances and azimuths, the acceleration amplitudes and displacement responses and their respective amplitude spectra are comparable. Furthermore, beating is observable in the responses of all three events. The beating effect period is computed using the relationship: $T_b=2T_1T_t/(T_1-T_t)$ given by Boroschek and Mahin (1991); however, in this case, to accurately quantify the period of the beating cycle is difficult since the translational and torsional frequencies are very close to one another. To provide a range of sample computations of beating frequency, (f_b) [period (T_b)], combinations of the translational frequency, f_1 (period, T_1), and the torsional frequency, f_t (period, T_t), are selected (Table 3). Computed beating periods provide a realistic range of beating periods that include those observed in most time-history plots throughout this paper, including Figure 15.

SITE RESPONSE AND RESONANCE

The spectra in Figure 16 computed using accelerations, in general, indicate significant peaks for the first three modes where, in most cases, the second modal peak amplitude is as large or larger than that of the fundamental mode. The significantly higher energy in the second structural mode is due to the closeness of the frequency of the second mode of the structure (for both NS and EW directions and for the second torsional mode) with that of the fundamental site frequency (1.3–1.8 Hz). Thus, in addition to the beating effect caused by closely coupled translational and torsional modes and compounded by low damping, the closeness of the frequency of the second modes (both NS

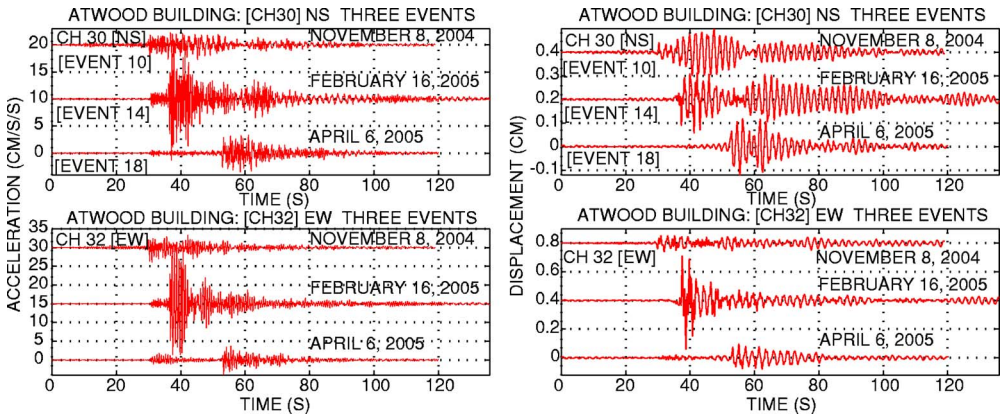

Figure 15. Acceleration and displacement time histories in the NS (CH30) and EW (CH32) directions at the roof for the three earthquakes that originate at varying distances and azimuths, all of which indicate a beating effect.

and EW) and that of the fundamental frequency of the site also contribute to the observed resonating responses. This is further corroborated in Figure 17, where it is seen that for all three events and for channel 30 (north-south at roof), in most cases, the energy of the second and third modes computed by the total record and the 40-second strong-shaking window of the response are higher (caused by beating and site resonance) when compared with the 40-second free-vibration window of the response (between 80 and 120 seconds into the record). Figure 18 shows that the observed (NS and EW) and computed site transfer functions compare very well for all three earthquakes. As previously (Figure 14), site transfer functions from observed data are computed as ratios of amplitude spectra.

CONCLUSIONS

An integrated structural and site response monitoring array at the Atwood Building in downtown Anchorage, Alaska, has recorded numerous small to medium earthquakes that occurred at near and far distances. It is expected that in the future, during stronger shaking, additional important data sets will be obtained. Detailed analysis of the data

Table 3. Range of beating frequency (fb) and period (Tb)

	Translational		Torsional		Beating	
	f_1 (Hz)	T_1 (s)	f_t (Hz)	T_t (s)	f_b (Hz)	T_b (s)
Case 1	0.55	1.8	0.6	1.66	0.023	42.7
Case 2	0.47	2.1	0.6	1.66	0.063	15.8
Case 3	0.47	2.1	0.55	1.82	0.037	27.3

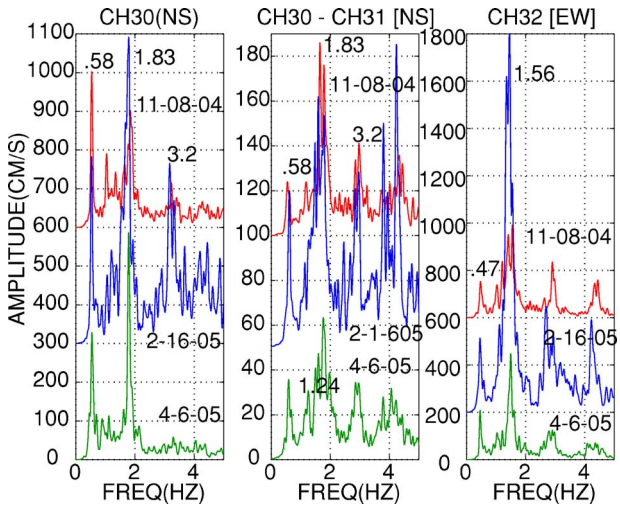

Figure 16. Amplitude spectra of accelerations (NS, EW, and torsional) at the roof for three earthquakes are similar in shape and consistently indicate larger peaks for second modes.

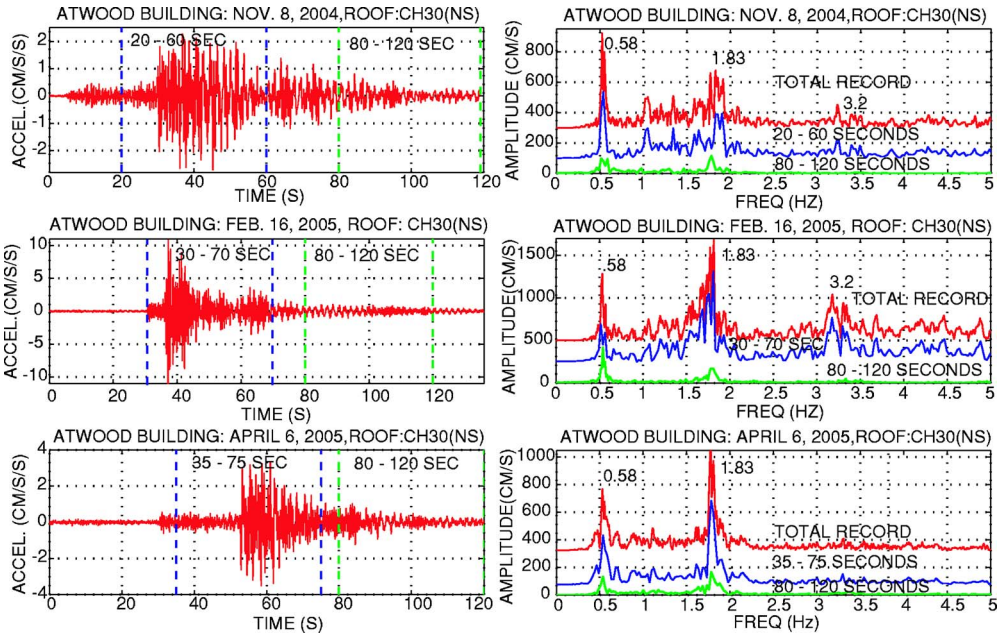

Figure 17. For each of the three events, north-south acceleration time history for roof (NS direction) and corresponding amplitude spectra for the total record and two 40-second windows, one during strong shaking and the other during free vibration. Compared to the first modal frequency, significant second modal peak amplitudes are observed.

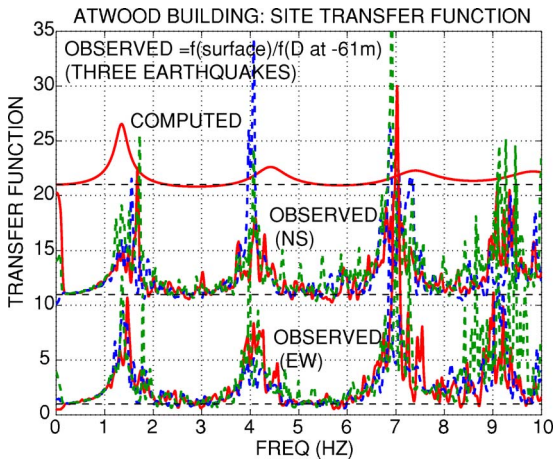

Figure 18. Comparison of computed transfer functions and those from ratios of amplitude spectra of NS and EW accelerations recorded at the surface and the deepest downhole for the three earthquakes indicates repeatability regardless of geographical origin of the three earthquakes.

from an earthquake that occurred at 186 km distance allowed computation of significant structural frequencies (e.g., fundamental mode NS 0.58 Hz and EW 0.47 Hz). Low damping percentages (2–4%) are identified. Torsional motions are closely coupled with translational motions as they exhibit similar frequencies and cause beating effects. Significant soil-structure interaction effects are not inferred from the data except that there is resonance due to the closeness of the second translational-torsional modes with that of the site fundamental site frequency, identified to be around 1.5 Hz from both the records and also from the transfer function computed with actual borehole data. Results related to dynamic characteristics, beating effect, site response, and resonance are repeated in three sets of data recorded from earthquakes that originate at different geographical distances and azimuths.

ACKNOWLEDGMENTS

Thanks to J. Steidl and U. Dutta for making some of the borehole data available. USGS-NSMP Data Center, managed by C. Stephens, diligently processes, stores, and disseminates the data. When processed and documented, all data is made available at http://nsmp.wr.usgs.gov.

REFERENCES

Bendat, J. S., and Piersol, A. G., 1980. *Engineering Applications of Correlation and Spectral Analyses*, John Wiley & Sons, New York, NY, 302 pp.

Boroschek, R. L., Mahin, S. A., and Zeris, C. A., 1990. Seismic response and analytical modeling of three instrumented buildings, *Proceedings, 4th U.S. National Conference on Earthquake Engineering, Palm Springs, Calif.*, vol. 2, pp. 219–228.

Boroschek, R. L., and Mahin, S. A., 1991. Investigation of the Seismic Response of a Lightly Damped Torsionally Coupled Building, Report *UCB/EERC-91/18*, Earthquake Engineering Research Center, University of California, Berkeley, 291 pp.

Çelebi, M., 2000. Seismic Instrumentation of Buildings, *U.S. Geol. Surv. Open-File Rep. 00-157*.

———, 2001. Current practice and guidelines for USGS instrumentation of buildings including federal buildings, in *COSMOS Proceedings, Invited Workshop on Strong-Motion Instrumentation of Buildings, Emeryville, Calif., November*, Cosmos Publication No. CP-2001/04.

———, 2003. Seismic Instrumentation Plan for Robert B. Atwood Building, Anchorage, AK 99501, Administrative Report, U.S. Geological Survey.

———, 2004a. Responses of a 14-story (Anchorage, Alaska) building to far-distance (M_w =7.9) Denali fault (2002) and near-distance earthquakes in 2002, *Earthquake Spectra* **20** (3), 693–706.

Çelebi, M., 2004b. Structural monitoring arrays—Past, present and future, *Proceedings, NATO Workshop on Future Directions on Strong Motion and Engineering Seismology, Kusadasi, Izmir, Turkey, May 17–21*, in Directions in Strong Motion Instrumentation, edited by P. Gulkan, and J. Anderson, NATO Science Series: IV. Earth and Environmental Sciences, Kluwer Academic Publishers, vol. 58, pp. 157–179.

Çelebi, M., Sanli, A., Sinclair, M., Gallant, S., and Radulescu, D., 2004. Real-time seismic monitoring needs of a building owner and the solution—A cooperative effort, *Earthquake Spectra* **19** (1), 1–23.

Ghanem, R., and Shinozuka, M., 1995. Structural System Identification—I: Theory, *J. Eng. Mech.* **121** (2), 255–264.

Haskell, N. A., 1953. The dispersion of surface waves on multi-layered media, *Bull. Seismol. Soc. Am.* **43** (1), 17–34.

———, 1960. Crustal reflection of plane SH waves, *J. Geophys. Res.* **65** (12), 4147–4150.

International Code Council (ICC), 2000. *International Building Code*, Whittier, CA.

Ljung, L., 1997. *System Identification—Theory for the User*, Prentice-Hall, Englewood Cliffs, NJ, 519 pp.

MathWorks, 1998 (and 1995 editions). User Guide: System Identification Toolbox for the User with Matlab, South Natick, MA, 200 pp.

Safak, E., 1999. Wave-propagation formulation of seismic response of multistory buildings, *J. Struct. Eng.* **125** (4), pp. 426–437.

Updike, R. G., and Carpenter, B. A., 1986. Engineering Geology of the Government Hill Area, Anchorage, Alaska, *U.S. Geol. Surv. Bull. 1588*, 36 pp.

Yang, Z., Dutpa, U., Çelebi, M., Liu, H., Biswas, N., Kono, T., and Benz, H., 2004. Strong motion instrumentation and structural response of Atwood Building in downtown Anchorage, Alaska, *Proceedings, 13 World Conference on Earthquake Engineering, Vancouver, B.C., Canada*. (CD-ROM)

(Received 21 November 2005; accepted 21 March 2006)